Supplementary Materials

Resetting amino acid metabolism of cancer cells by $ATB^{0,+}$-targeted nanoparticles for enhanced anticancer therapy

Longfa Kou[1,#], Xinyu Jiang[1,2,#], Yingying Tang[1], Xing Xia[1], Yingtao Li[1,3], Aimin Cai[1], Hailun Zheng[1], Hailin Zhang[1,3], Vadivel Ganapathy[1,4], Qing Yao[1,2,*], Ruijie Chen[1,*]

[1] Department of Pharmacy, The Second Affiliated Hospital and Yuying Children's Hospital of Wenzhou Medical University, Wenzhou 325027, China

[2] School of Pharmaceutical Sciences, Wenzhou Medical University, Wenzhou 325035, China

[3] Department of Children's Respiration Disease, The Second Affiliated Hospital and Yuying Children's Hospital of Wenzhou Medical University, Wenzhou 325027, China

[4] Department of Cell Biology and Biochemistry, Texas Tech University Health Sciences Center, Lubbock, TX 79430, USA

[#] These authors contributed equally to this work.

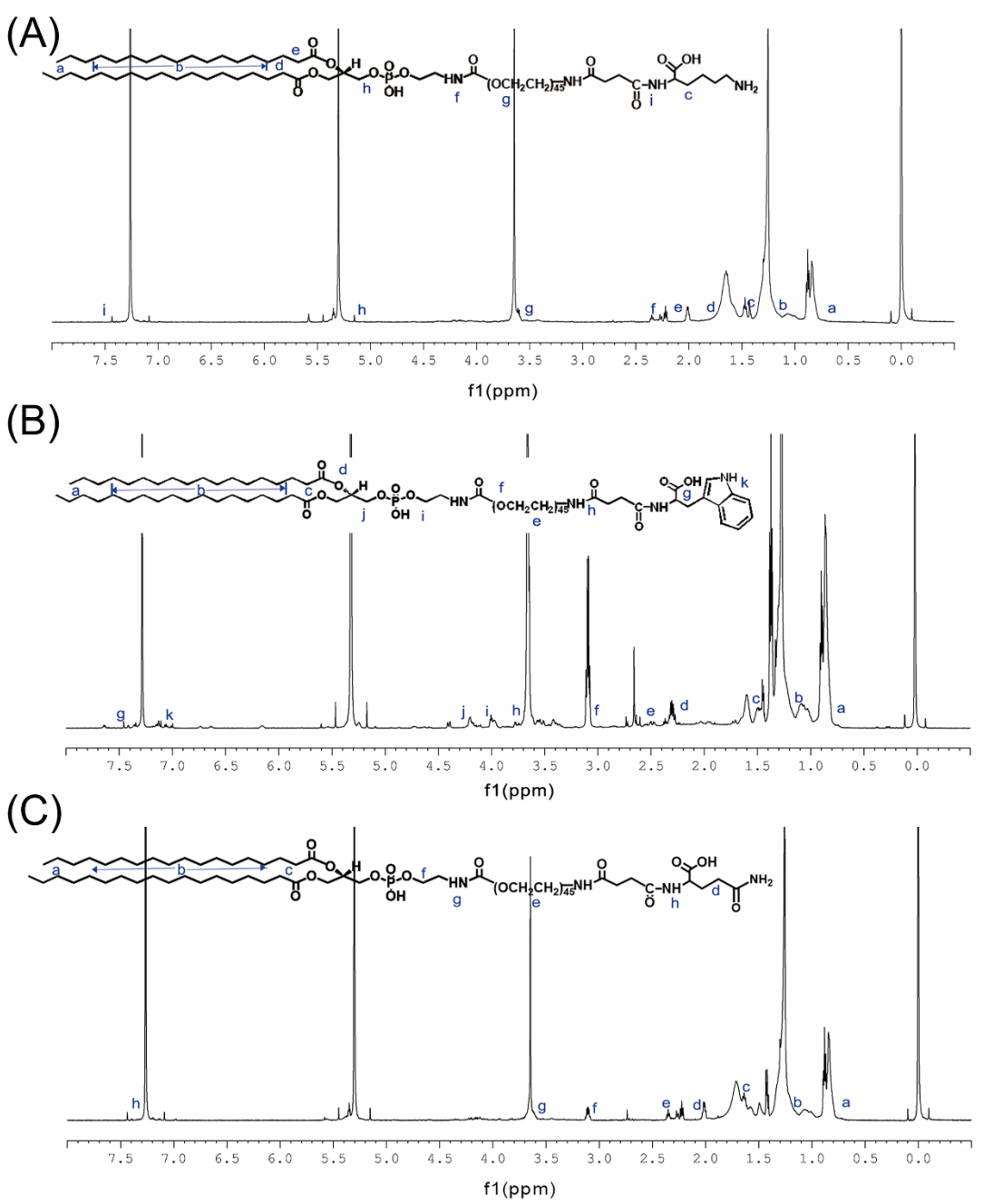

Fig. S1. ^{1}H NMR spectra of (A) DSPE-PEG2000-Lysine, (B) DSPE-PEG2000-tryptophan, and (C) DSPE-PEG2000-glutamine in $CDCl_3$.

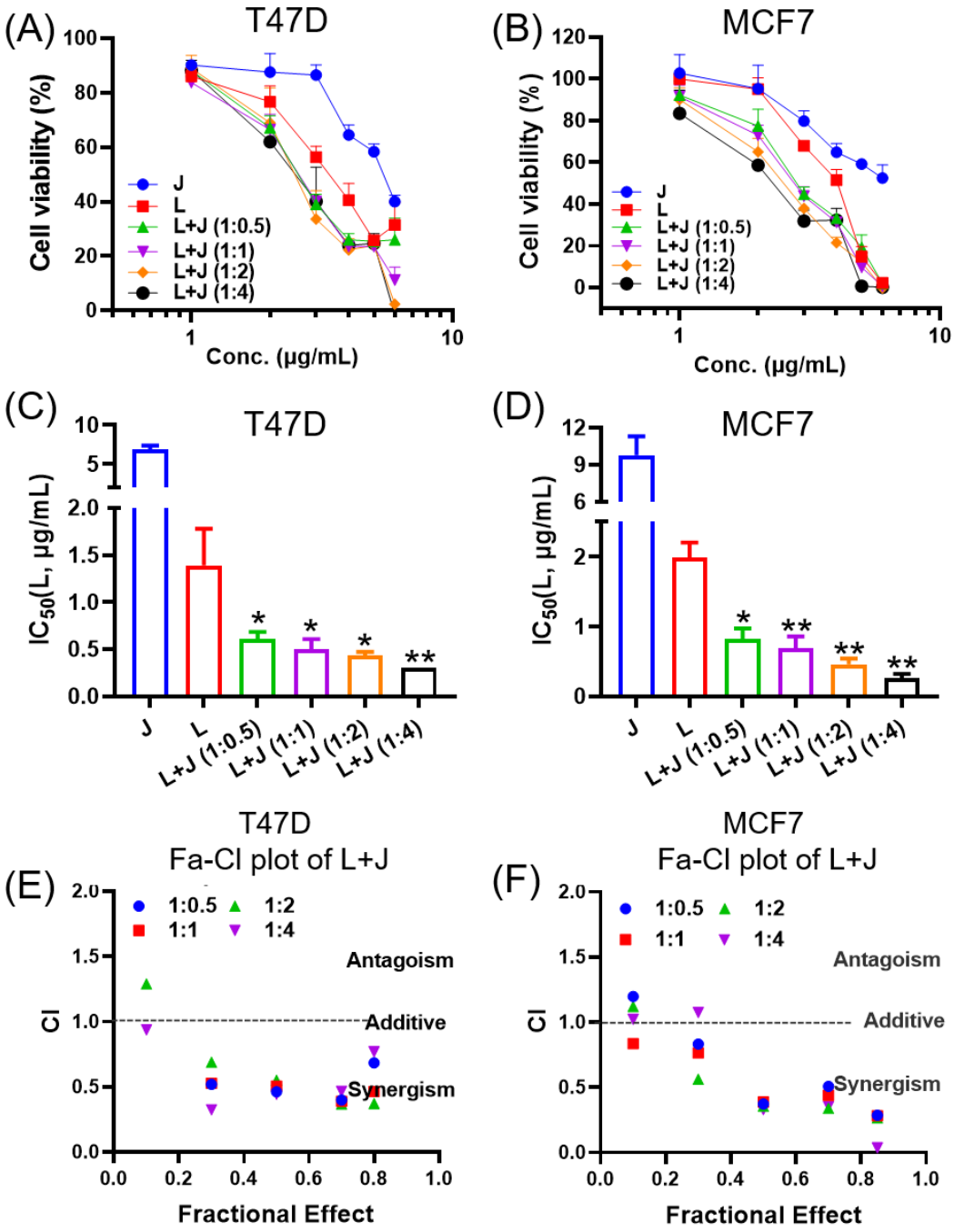

Fig. S2. The relative cell viabilities of (A) T47D and (B) MCF7 cells after lapatinib (L) and JPH203 (J) combined treatment with various ratios. The IC_{50} value of L in (C) T47D and (D) MCF7 cells in the combined treatments. Fa-CI plot of L+J at different combined ratios in (E) T47D and (F) MCF7 cells. Data represent means ± SD (n = 6). *, $p < 0.1$, **, $p < 0.05$, compared to the control group.

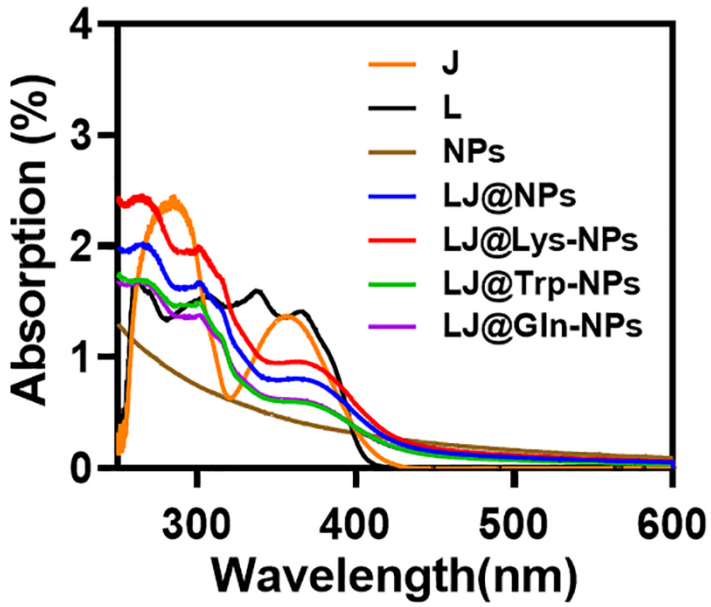

Fig. S3. The UV-VIS absorption spectrum of JPH203, lapatinib, blank NPs and drug-loaded nanoparticles.

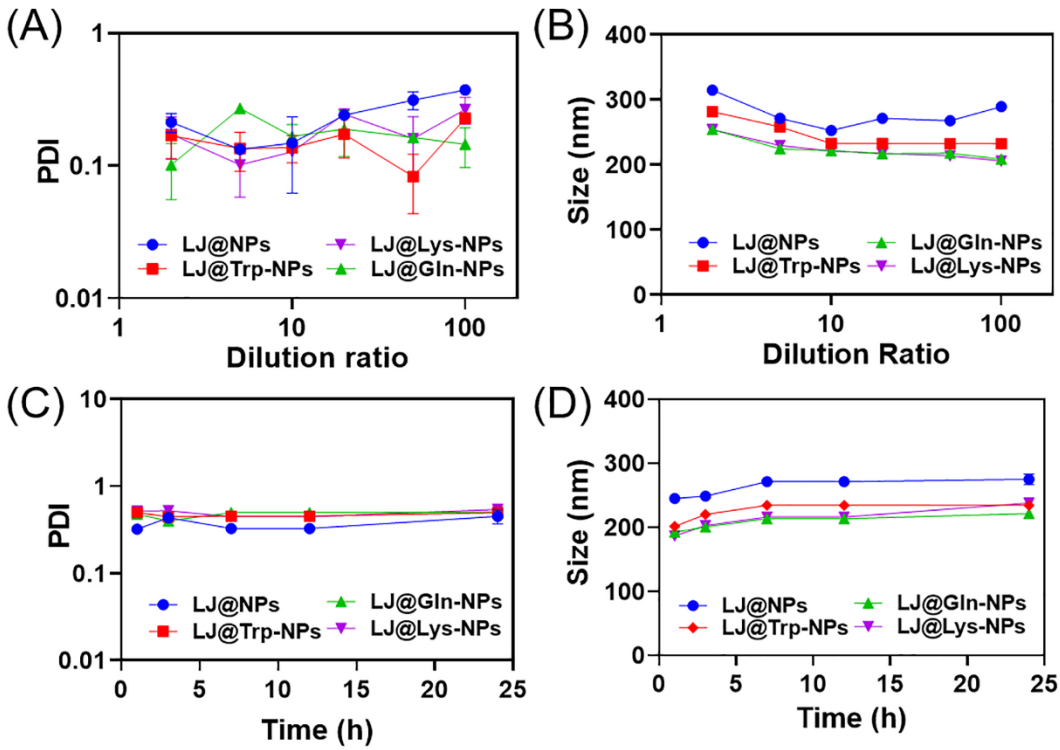

Fig. S4. The dilution stability of LJ@-NP, LJ@Trp-NP, LJ@Gln-NP, LJ@Lys-NP presented by the changes in (A) polydispersity index (PDI) and (B) particle size. Stability of (C) polydispersity index (PDI) and (D) particle size after incubation of the various formulations with a serum-containing solution (10%) at 37 °C. Data represent means ± SD (n = 3).

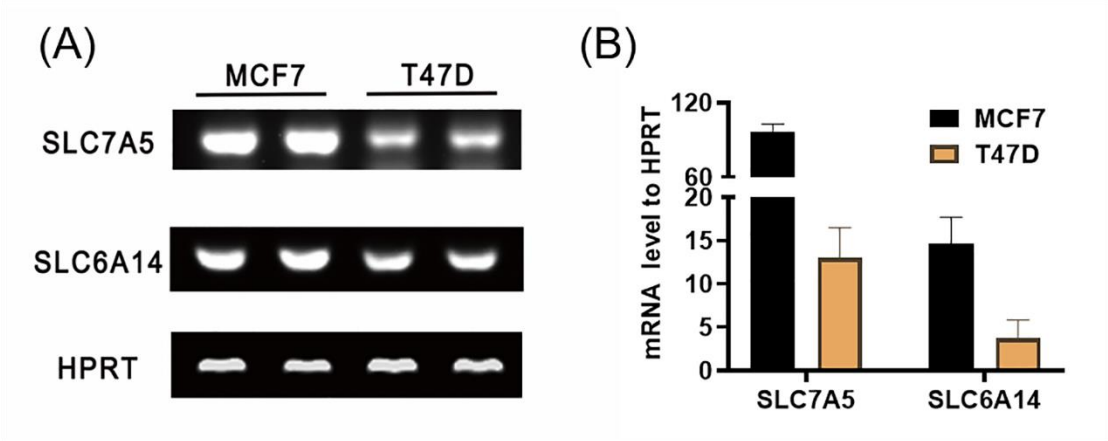

Fig. S5. (A) SLC7A5 and SLC6A14 mRNA expression (semi-quantitative) in MCF7 cells and T47D cells. (B) qPCR for SLC7A5 and SLC6A14 mRNA expression. Data represent means ± SD, n=3.

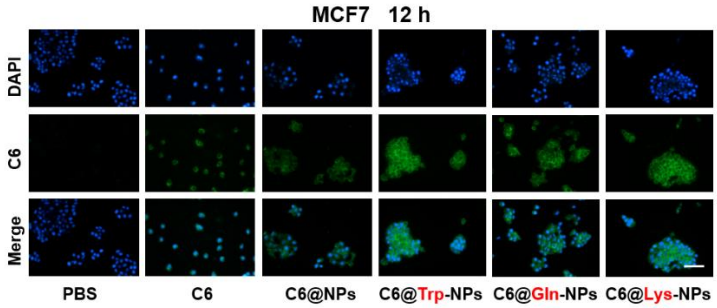

Fig. S6. Fluorescence images for the uptake of free C6, C6@NP, C6@Trp-NP, C6@Gln-NP, C6@Lys-NP in MCF7 cells after 12 h incubation (Scale bar = 50 μm).

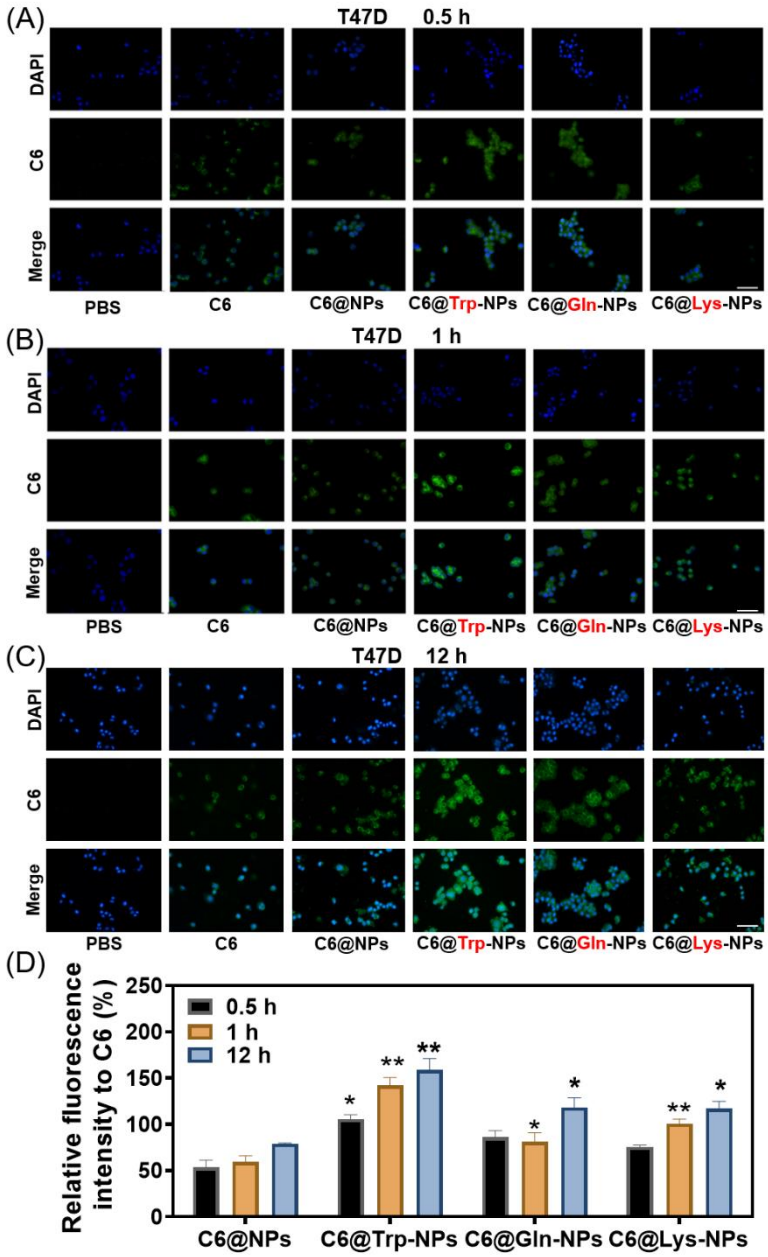

Fig. S7. Fluorescence images for the uptake of free C6, C6@NP, C6@Trp-NP, C6@Gln-NP, C6@Lys-NP in T47D cells after (A) 0.5 h, (B) 1 h, and (C) 12 h incubation. C6 (green) was used as the fluorescence probe, and DAPI (blue) was used for nuclei localization. Scale bar = 50 μm. (D) Quantitative analysis of the intracellular NPs uptake. Data represent means ± SD, n=3. *, $p<0.05$, compared to C6@NPs group.

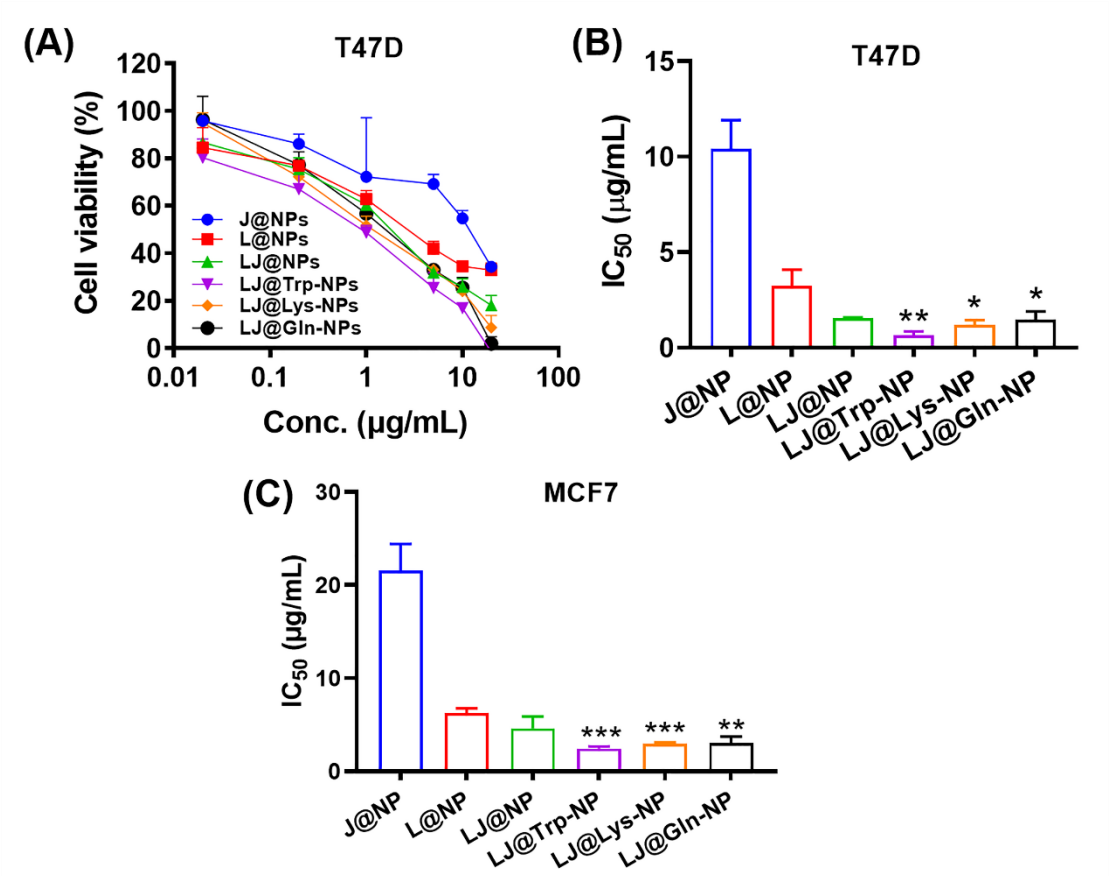

Fig. S8. Viability of T47D cells after NPs treatments (A), and the respective IC_{50} values (B). The IC_{50} value of different formulations in MCF7 cells (C). Data represent means ± SD, n=3. *, $p<0.05$, **, $p<0.01$, ***, $p<0.001$, compared to the control group.

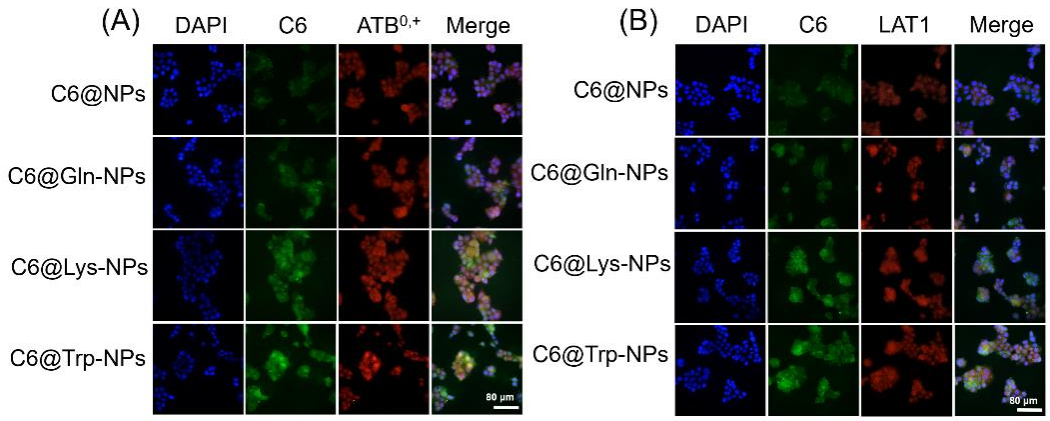

Fig. S9. Colocalization study of NPs with (A) $ATB^{0,+}$ or (B) LAT1 in MCF7 cells after 1 h incubation. Blue: DAPI stained nuclei; Green: C6-labelled NPs; Red: $ATB^{0,+}$ or LAT1. Scale bar: 80 μm.

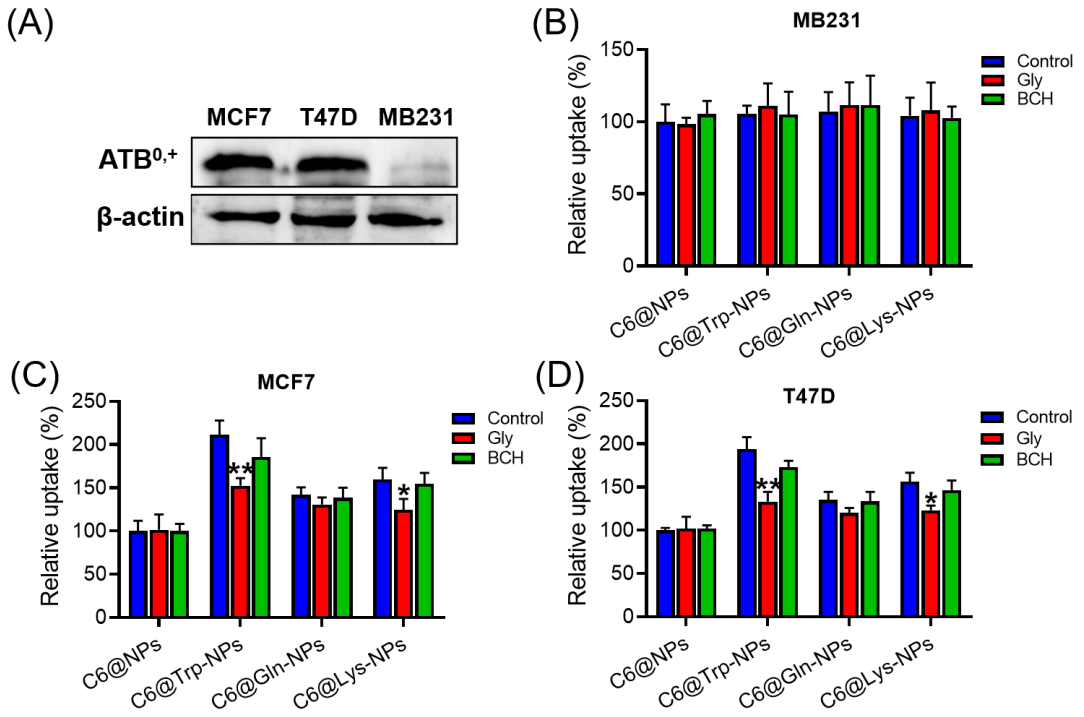

Fig. S10. (A) The expression of $ATB^{0,+}$ in MCF7, T47D, and MB231 cells. The uptake of C6@NP, C6@Trp-NP, C6@Gln-NP, C6@Lys-NP in (B) MB231, (C) MCF7, and (D) T47D cells in the presence of glycine (Gly, 1 mM) or BCH (1 mM). Data represent means ± SD, n=3. *, $p<0.05$, **, $p<0.01$, compared to the control group.

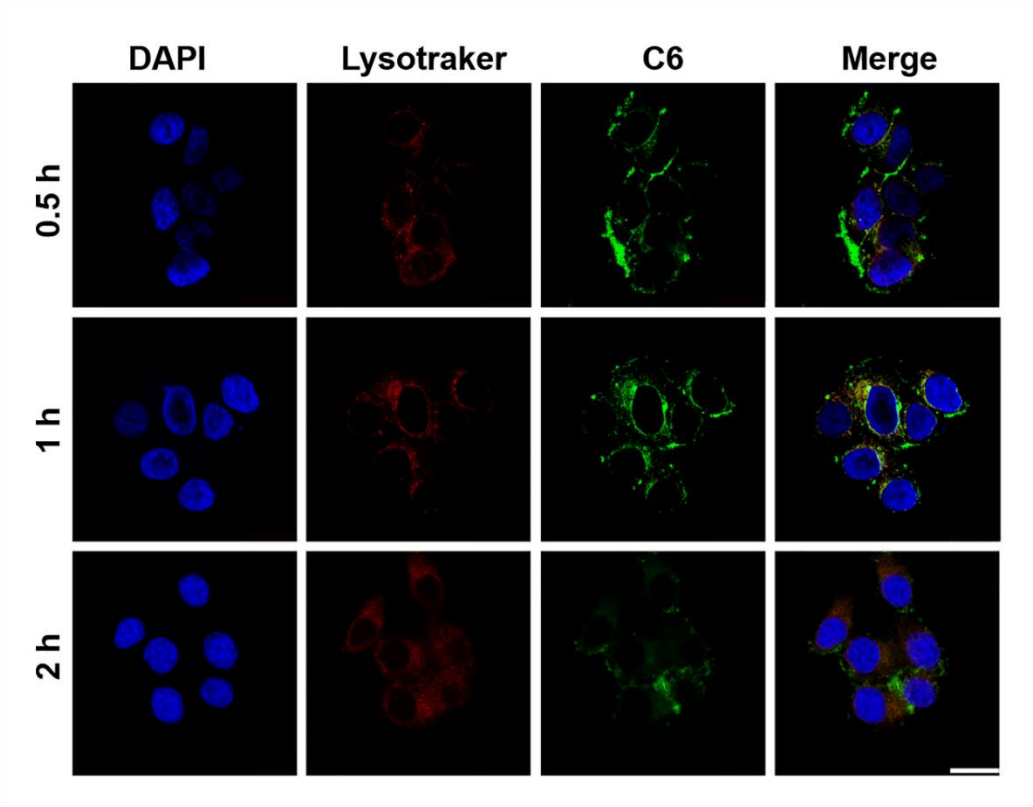

Fig. S11. Intracellular traffic of C6@Trp-NPs examined by confocal laser scanning microscope

(CLSM). MCF7 cells were incubated with C6@Trp-NPs for 0.5 h, and then the nanoparticles were removed. Fresh medium was added for another 1 h and 2h incubation. In each treatment, C6 concentration was fixed at 4 μg/mL. Lysosomes and nuclei were stained with LysoTracker (Red) and DAPI (blue), respectively. Scale bar = 20 μm.

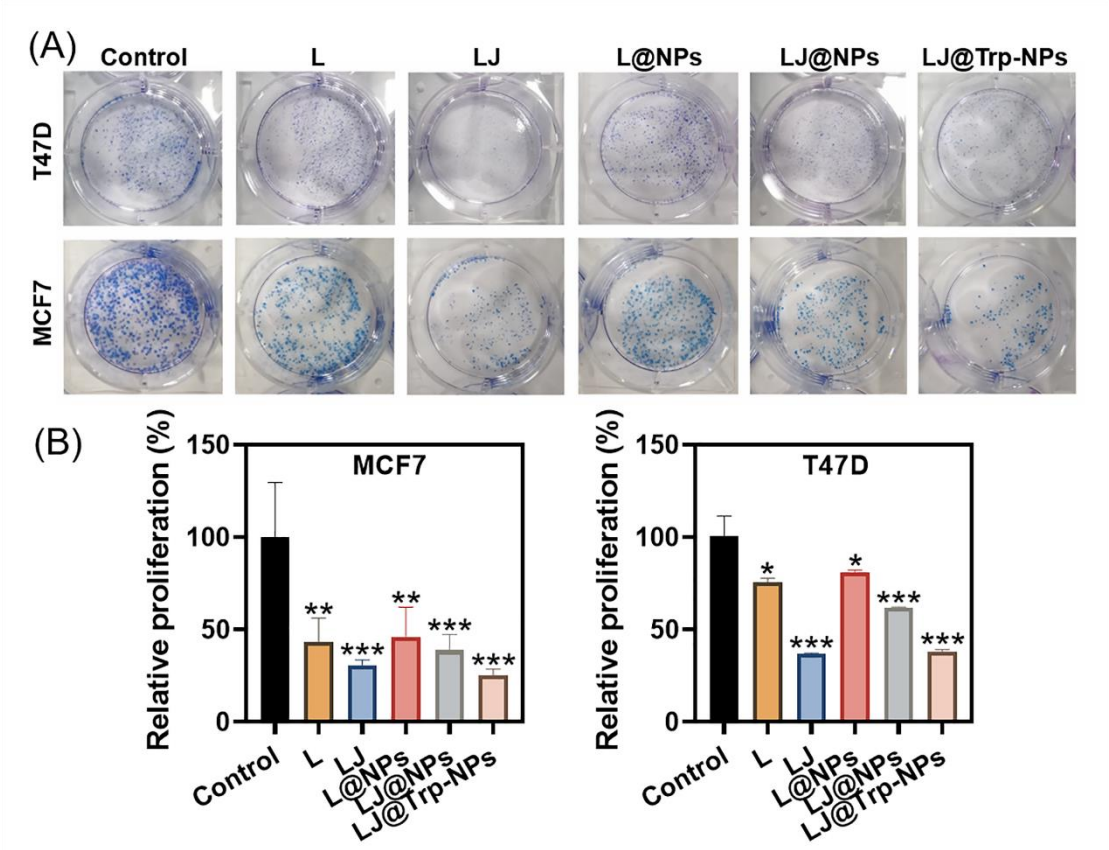

Fig. S12. (A) Colony formation assay in MCF7 and T47D cells after various treatments. (B) Quantitative analysis of the colony numbers. Data represent means ± SD, n=3. *, $p<0.05$, **, $p<0.01$, ***, $p<0.001$, compared to the control group.

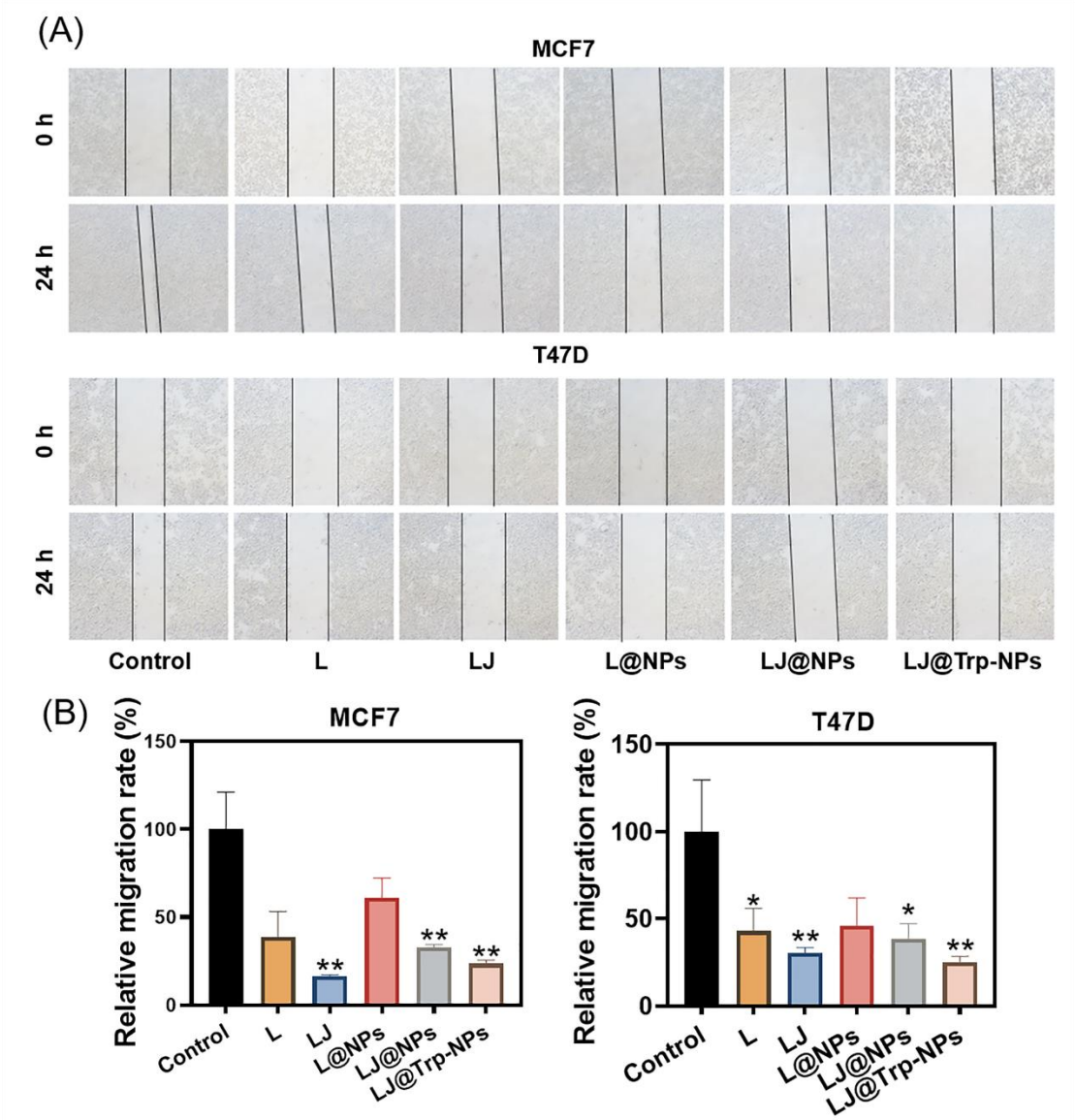

Fig. S13. (A) Wound healing assay with different treatments. (B) The migration rate in the experimental group was calculated compared to the control group. *, $p<0.05$, **, $p<0.01$, compared to the control group.

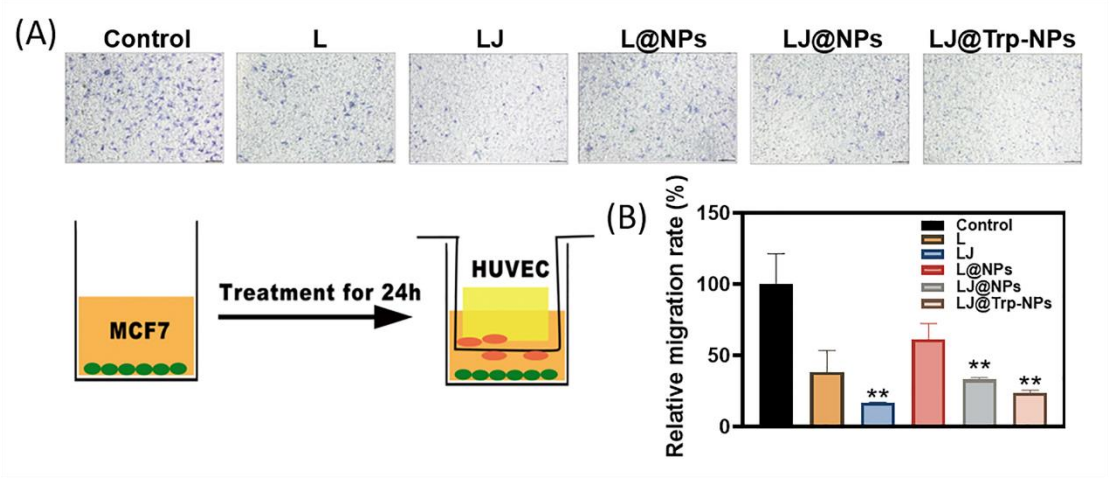

Fig. S14. (A) Representative images (upper panels) and schematic diagram of transwell migration of HUVECs (lower left panel) co-cultured with MCF7 cells treated with different formulations. (B) Quantitative analysis for HUVEC migration. Scale bar = 100 μm. **, $p<0.01$.

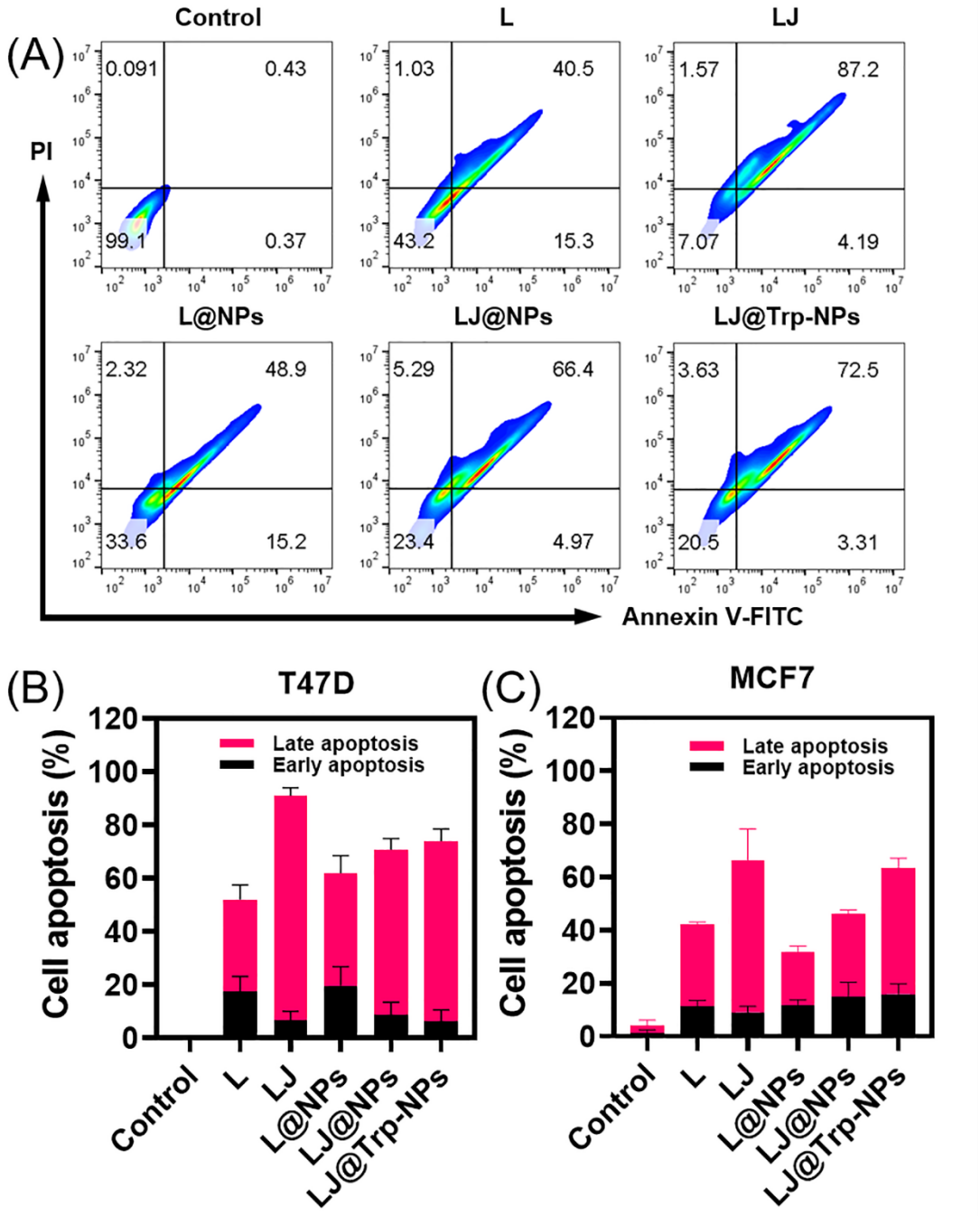

Fig. S15. (A) Apoptosis analysis in T47D cells using flow cytometry. Histogram showing the percentage of apoptotic cells after various treatments in (B) T47D cells and (C) MCF7 cells. Data present means ± SD (n=3).

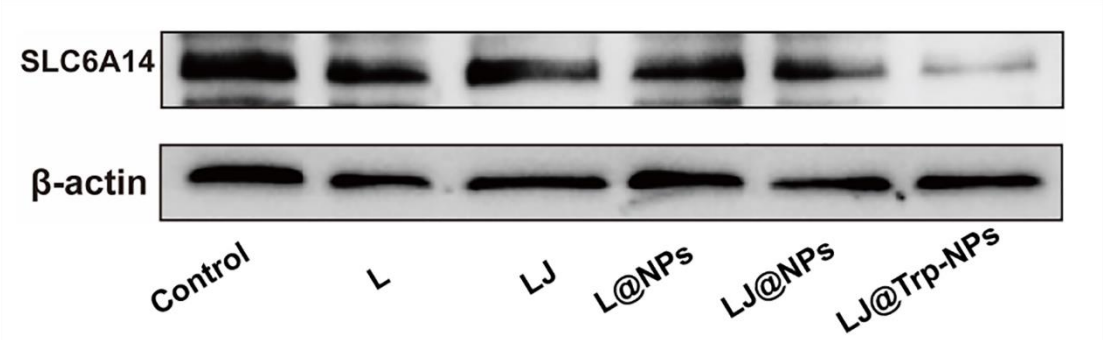

Fig. S16. Expression pattern of SLC6A14 protein in MCF7 cells after treatment with various formulations for 24 h as assessed by Western blot.

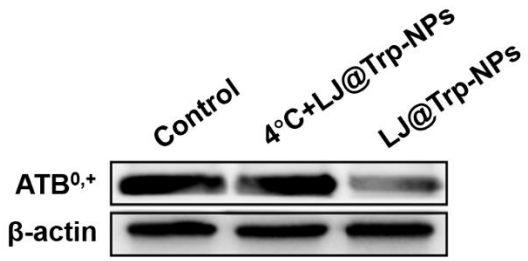

Fig. S17. The expression of $ATB^{0,+}$ in MCF7 cells after incubation with LJ@Trp-NPs at 4 °C and 37 °C.

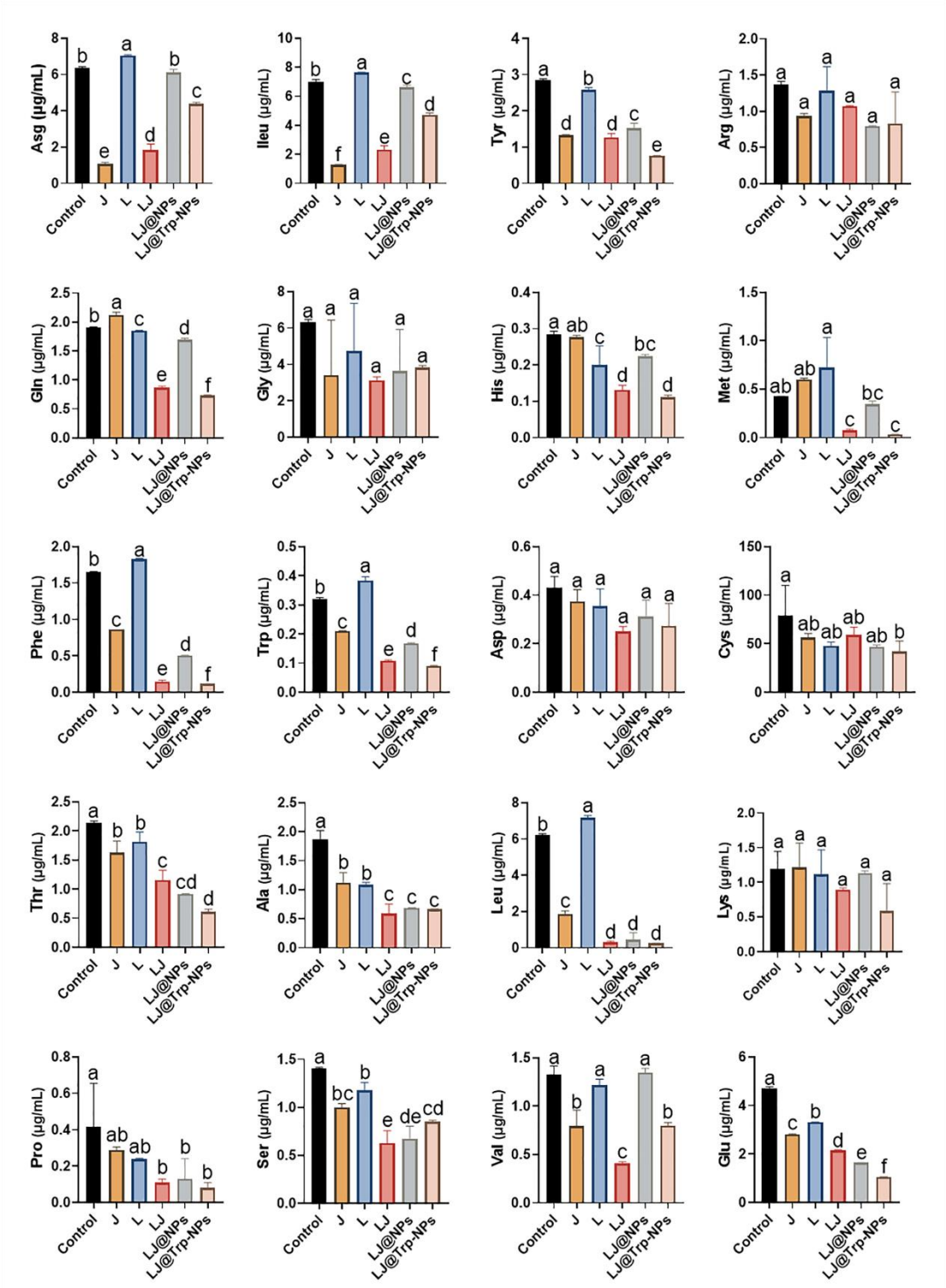

Fig. S18. Quantitative analysis of intracellular proteinogenic amino acids in MCF7 cells after treatment with various formulations. The different letters above the bars indicate statistically significant differences ($P < 0.05$) among the values in the bars.

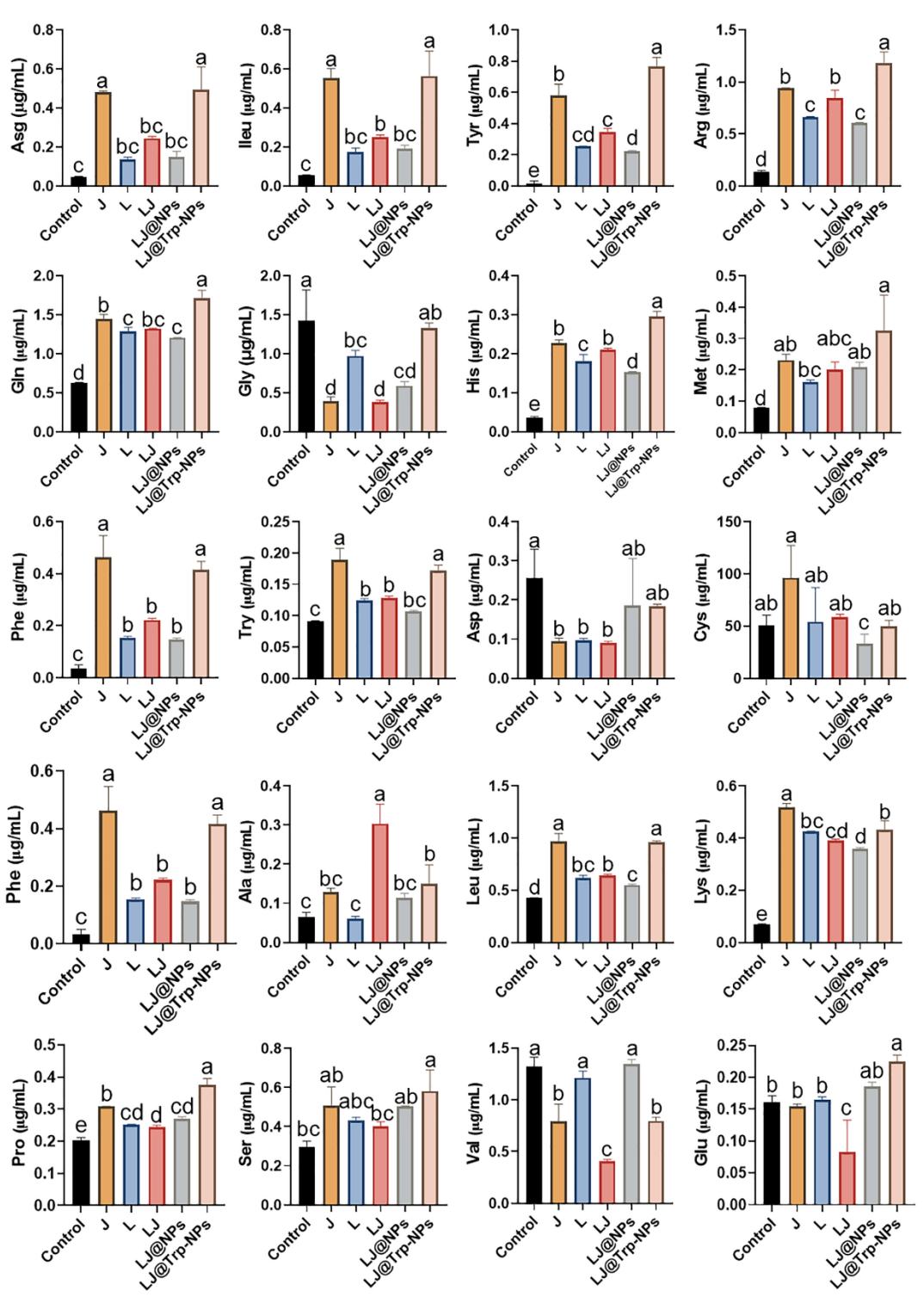

Fig. S19. Quantitative analysis of extracellular proteinogenic amino acids in MCF7 cells after treatment with various formulations. The different letters above the bars indicate statistically significant differences ($P < 0.05$) among the values in the bars.

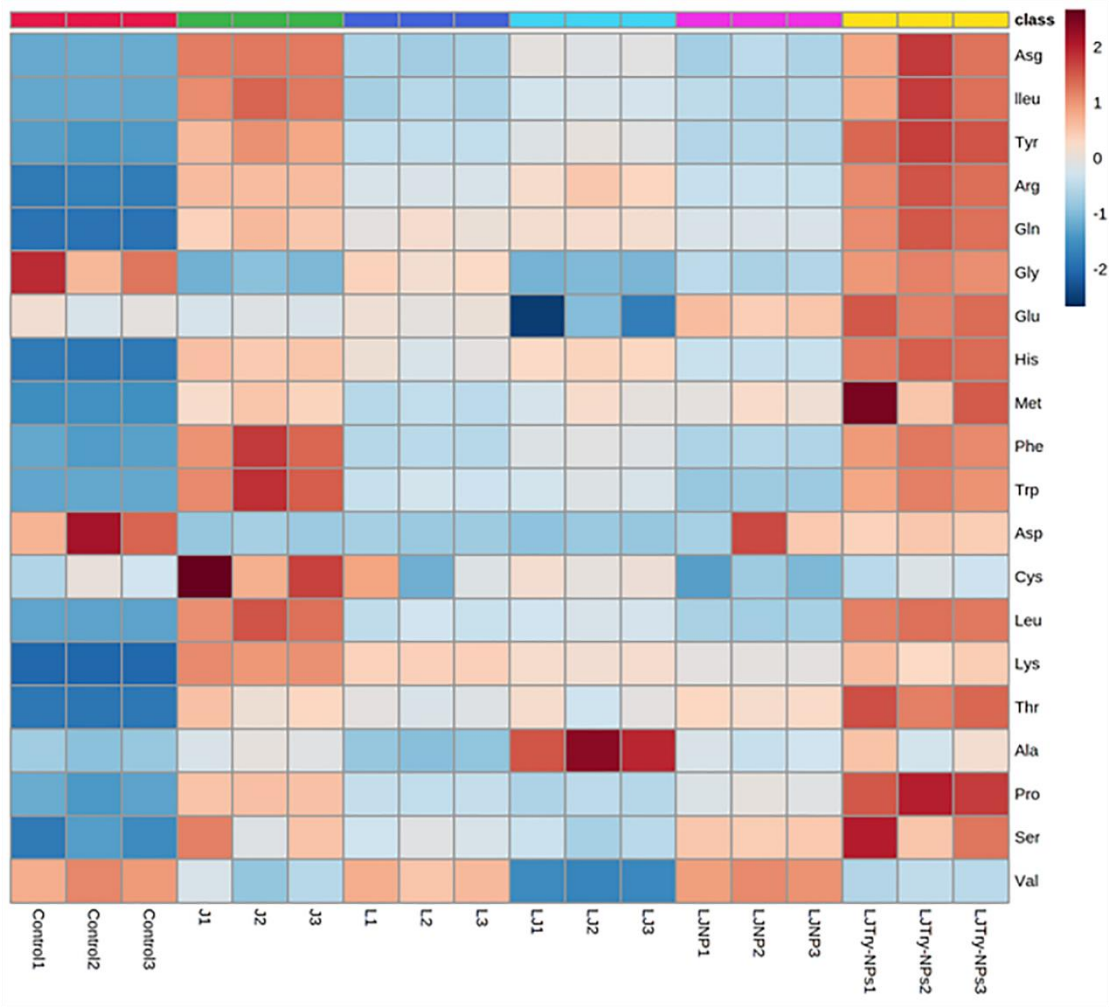

Fig. S20. Heatmap of extracellular amino acid content in MCF7 cells treated with different formulations.

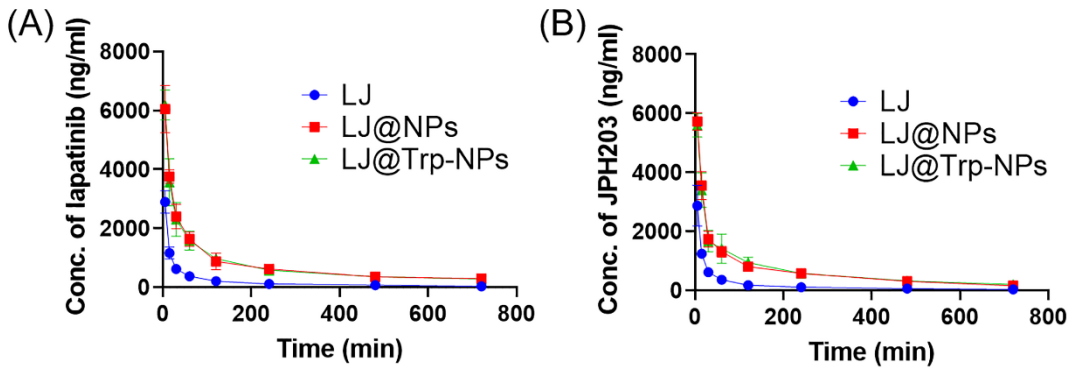

Fig. S21. The pharmacokinetic profiles of (A) lapatinib and (B) JPH203 in free LJ, LJ@NPs, LJ@Trp-NP. Data represent means ± SD (n=3).

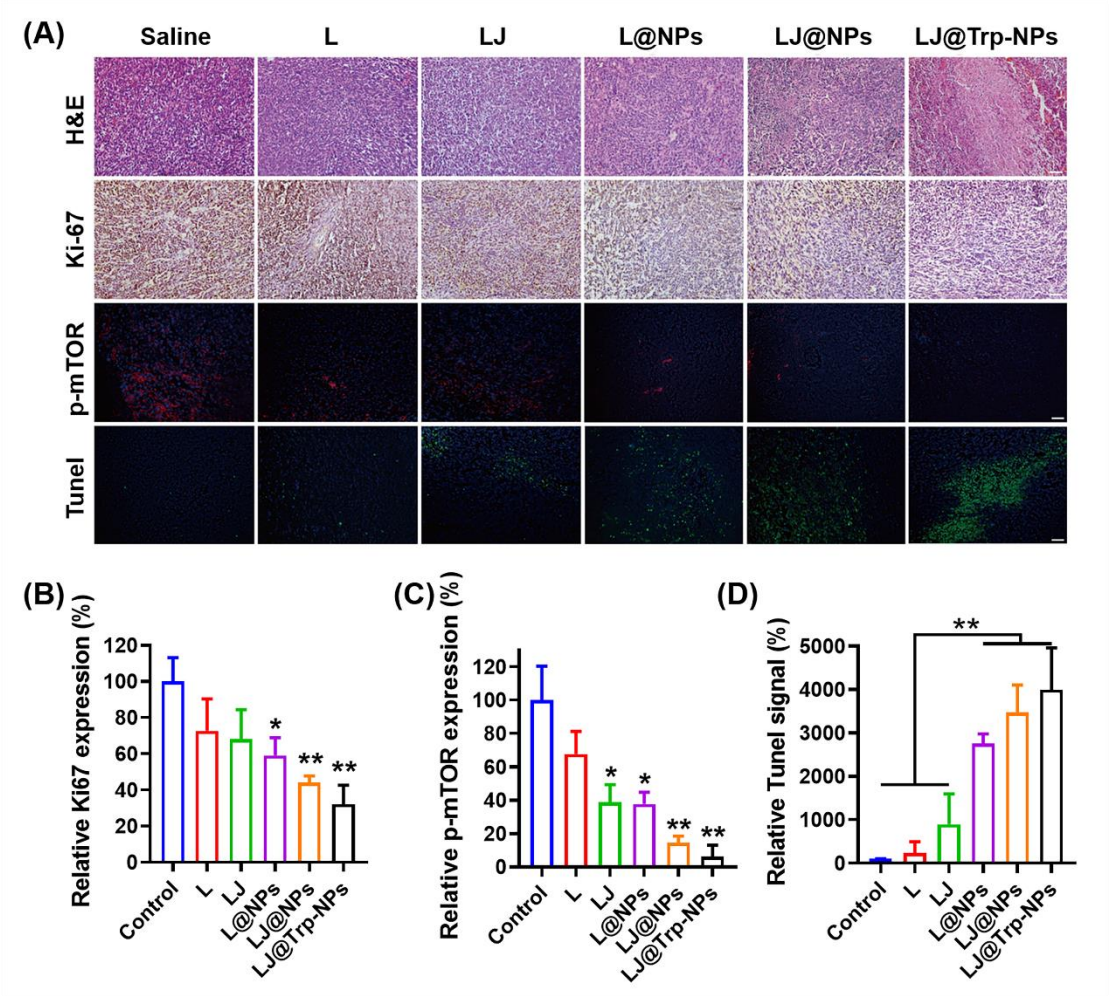

Fig. S22. The histological analysis of tumor tissue after different treatments. (A) Hematoxylin and eosin (H&E) staining, immunohistochemical staining for Ki 67, immunofluorescence staining for p-mTOR, and TUNEL analysis of tumor tissue in different groups (Scale bar = 50 μm). Quantitative analysis of (B) Ki67 expression, (C) p-mTOR, and (D) TUNEL signal. Data are presented as means ± SD, n=6.

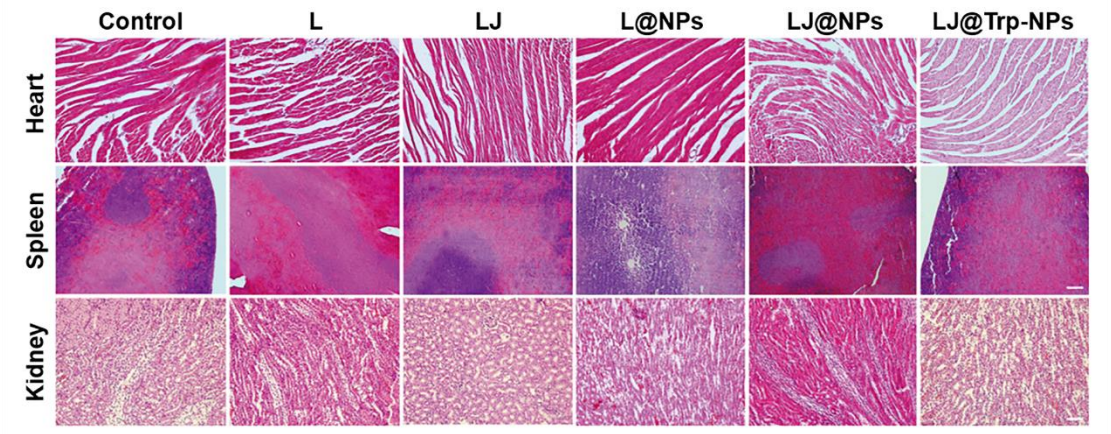

Fig. S23. Representative H&E staining of heart, spleen, kidney sections from each group (Scale

bar = 50 μm).

Table S1. Physicochemical properties of lapatinib (L)- and JPH203 (J)-coloaded nanoparticles.

Nanoparticles	Size (nm)	PDI	Potential (mV)	EE of L (%)	DL of L (%)	EE of J (%)	DL of J (%)	Yield (%)
LJ@NPs	152.25±1.91	0.064±0.003	-15.30±0.71	85.46±3.14	4.69±0.35	70.81±4.47	4.15±0.38	85.1±4.1
LJ@Lys-NPs	154.15±1.48	0.039±0.023	-2.41±0.17	85.85±5.97	4.68±0.22	76.87±6.45	4.27±0.09	84.9±6.2
LJ@Trp-NPs	181.25±0.92	0.043±0.009	-1.65±0.14	81.28±6.96	4.67±0.10	76.32±9.61	4.33±0.33	81.3±6.8
LJ@Gln-NPs	136.9±1.27	0.055±0.006	-3.70±0.19	79.69±0.85	4.67±0.38	81.91±6.32	4.41±0.35	83.3±4.5

Data were represented as mean ± SD (n = 3).

Table S2. The pharmacokinetic parameters of free lapatinib and lapatinib-loaded liposomes in rats (n=3).

	AUC_{0-t} (μg·min·ml^{-1})	$AUC_{0-\infty}$ (μg·min·ml^{-1})	$t_{1/2}$ (min)	CL (ml/min)
LJ	122.9±11.0	127.3±12.5	93.6±13.0	39.5±3.7
LJ@NPs	518.1±41.2	673.2±99.1	351.5±97.7	7.5±1.2
LJ@Trp-NPs	512.9±93.6	670.7±64.3	380.1±99.9	7.5±0.7

Table S3. The pharmacokinetic parameters of free JPH203 and JPH203-loaded liposomes in rats (n=3).

	AUC_{0-t} (μg·min·ml^{-1})	$AUC_{0-\infty}$ (μg·min·ml^{-1})	$t_{1/2}$ (min)	CL (ml/min)
LJ	115.1±14.3	119.2±14.3	74.4±25.2	42.4±5.4
LJ@NPs	439.4±36.3	514.9±79.1	308.4±89.5	9.9±1.6
LJ@Trp-NPs	462.1±17.8	554.2±33.4	291.6±81.4	9.0±0.6